

# Seismic Behavior of Self-Centering Modular Panel with Slit Steel Plate Shear Walls: Experimental Testing

Wei Wang<sup>1</sup>; Jianhong Kong<sup>2</sup>; Yunfeng Zhang<sup>3</sup>; Gongling Chu<sup>4</sup>; and Yiyi Chen<sup>5</sup>

**Abstract:** The self-centering modular panel with a slit steel plate shear wall (SCMP-SW) is a new seismic load-resisting structural component that combines recentering capabilities and energy dissipation ability. The self-centering modular panel is designed as a posttensioned steel moment resisting frame and in this study two types of SCMP-SWs with slightly different configurations are fabricated and tested, which could be potentially inserted into framed structural systems. In this paper, the prefabricated SCMP-SW is installed into a beam-through steel frame, while the slit wall is intended to serve as replaceable fuse elements for energy dissipation purposes. A series of experimental tests were conducted to investigate the cyclic loading behavior of the SCMP-SW with two different types of self-centering modular panels and slit walls. The experimental results show that SCMP-SW is capable of recentering upon unloading while retaining the moderate energy-dissipation capacity of the slit walls. It is also observed that due to the self-centering modular panel, after severe cyclic loading the system with newly replaced slit walls and a reused main frame exhibits almost identical structural performance (stiffness, strength, and recentering ability) to the original system. DOI: 10.1061/(ASCE)ST.1943-541X.0001932. © 2017 American Society of Civil Engineers.

**Author keywords:** Self-centering; Modular panel; Rocking connection; Slit wall; Experiment; Seismic effects.

## Introduction

Slit steel plate shear walls (SWs), referred to simply as *slit walls*, are a new type of earthquake-resisting element (Hitaka and Matsui 2003). The idea of using slits in shear walls is traced back to earlier studies by Omori et al. (1966) and Mutoh et al. (1968), who proposed using slits to improve the earthquake resistance of reinforced concrete shear walls. The basic concept of these walls is for the steel plate segments between the vertical slits to behave as a series of flexural links, which undergo large flexural deformations relative to their shear deformation and provide a fairly ductile response without the need for heavy stiffening of the wall. Energy dissipation is provided primarily through yielding at the top and bottom of the flexural links. Compared with conventional steel plate shear walls, the slit walls have following two features (Hitaka and Matsui 2003):

1. Strength and stiffness of the slit walls can be adjusted more easily by changing the slit configuration (interval, length, and number of layers of slits); and

2. The slit walls are compact and need not occupy the full beam span, thus accommodating door or window openings adjacent to the wall.

When subjected to severe earthquake loading, the conventional seismic lateral-force-resisting system with slit walls can develop inelastic deformations in slit walls and primary structural members. Structural damage associated with these inelastic deformations may be impractical to repair after an earthquake, especially when coupled with permanent residual drifts.

In order to reduce postearthquake structural repair workload and thereby mitigate economic and functionality losses, self-centering systems have been developed to bring a structural system back to a fully functional state following an earthquake. These systems typically use rocking posttensioned (PT) members to provide the restoring forces required to return a building to its original position. This concept was originally implemented in unbonded posttensioned precast concrete walls and frames in the early 1990s (Priestly 1991; El-Sheikh et al. 1999; Kurama et al. 1999) and later extended to posttensioned steel moment resisting frames in the early 2000s (Garlock 2002). The PT steel moment resisting frames typically consist of columns and beams, with high-strength steel bars or strands placed within the depth of the beams and anchored to the outer flanges of the columns. The PT beam-to-column connections can be used to provide a frame with self-centering capacity and limit damage to replaceable energy-dissipating elements (e.g., Ricles et al. 2002; Christopoulos et al. 2002a, b; Garlock et al. 2005; Rojas et al. 2005). During lateral sway, the PT connections rock about the beam flanges, the initiation of which is referred to as connection decompression, causing the PT elements to elongate, thus producing the restoring forces necessary to recenter the building (Garlock et al. 2007). Based on this concept, the self-centering steel plate shear walls (SC-SPSWs), which feature thin web plates and PT connections between the beams and columns, have been investigated by Dowden et al. (2012), Clayton et al. (2012a, b, 2013, 2016), and Clayton (2013). This system combines the advantages of high lateral stiffness and energy-dissipation capacity from the thin web plates, and self-centering capability

<sup>1</sup>Professor, State Key Laboratory of Disaster Reduction in Civil Engineering, Dept. of Structural Engineering, Tongji Univ., Shanghai 200092, China. E-mail: weiwang@tongji.edu.cn

<sup>2</sup>Graduate Student, Dept. of Structural Engineering, Tongji Univ., Shanghai 200092, China.

<sup>3</sup>Professor, Dept. of Civil and Environmental Engineering, Univ. of Maryland, College Park, MD 20742 (corresponding author). E-mail: zyzf@umd.edu

<sup>4</sup>Ph.D. Student, Dept. of Structural Engineering, Tongji Univ., Shanghai 200092, China.

<sup>5</sup>Professor, State Key Laboratory of Disaster Reduction in Civil Engineering, Dept. of Structural Engineering, Tongji Univ., Shanghai 200092, China.

Note. This manuscript was submitted on March 9, 2017; approved on July 6, 2017; published online on November 10, 2017. Discussion period open until April 10, 2018; separate discussions must be submitted for individual papers. This paper is part of the *Journal of Structural Engineering*, © ASCE, ISSN 0733-9445.

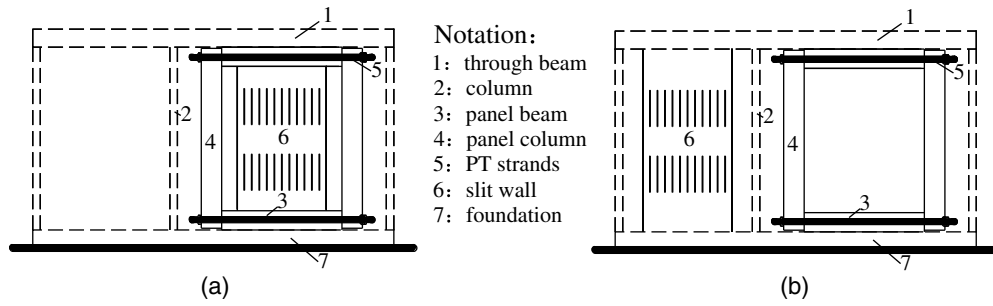


Fig. 1. Typical elevation arrangement of SCMP-SW: (a) integrated type; (b) separated type

from the PT connections. In recent years, alternative self-centering solutions based on shape memory alloys (SMAs) and energy-dissipation solutions based on stainless steel links have also received attention (Fang et al. 2014, 2015, 2017; Wang et al. 2015a, b, 2016a, b).

Based on the previous research on self-centering modular panels (SCMPs) (Wang et al. 2017), this paper presents a new type of seismic load-resisting structural component termed *self-centering modular panel with a slit wall*, abbreviated as SCMP-SW. The SCMP-SWs concerned in this study have two types of configurations with different arrangements of the two key components, SCMP and SW. The SCMP is composed of panel beams, panel columns, and PT strands. Fig. 1(a) shows the elevation view of the first integrated type of SCMP-SW used in a structural system termed *beam-through steel frame* (Wang et al. 2013, 2016a, b), in which the integrated type of SCMP-SW is shown in solid lines and the main frame is shown in dashed lines. If the second separated type of SCMP-SW is used in the main frame, a slit wall is placed in the bay in which the SCMP is not placed. Owing to the PT connections, the SCMP has the self-centering ability upon unloading, thus can recenter the whole structural system after earthquakes. The SCMP-SW can be shop fabricated and then transported to the construction site for rapid installation into a framed structural system through bolted connections to the frame beam.

In conclusion, SCMP-SW can be designed to combine the lateral force resistance and self-centering ability. This paper presents an experimental program in which the SCMP-SW was installed into a beam-through steel frame in order to investigate the SCMP-SW behavior under cyclic lateral loads, including system response, SCMP-SW (including the two types mentioned previously) response, and their interaction.

## Theoretical Behavior of SCMP-SW

### SCMP-SW Forces

Upon lateral loading, the main frame beam transfers lateral forces to the SCMP-SW through high-strength bolted connections near both panel-beam ends, making the SCMP-SW change from a rectangle to a parallelogram once gaps open. To understand the SCMP-SW behavior, the free-body diagram of the integrated type of SCMP-SW in its deformed shape can be used (Fig. 2), in which  $F_B$ ,  $V_B$ , and  $M_B$  are the lateral forces, vertical forces, and moments between the main frame beams and panel beams, respectively;  $T_{PT}$  is the resultant force of the PT strands at each connection;  $F_{SW}$  and  $V_{SW}$  are the lateral forces and vertical forces between the panel beams and slit walls, respectively;  $H_{SCMP}$  is the overall height of SCMP; and  $\theta_r$  is the gap opening angle. The PT elements and slit walls are not shown for clarity in Fig. 2. The slit walls are only

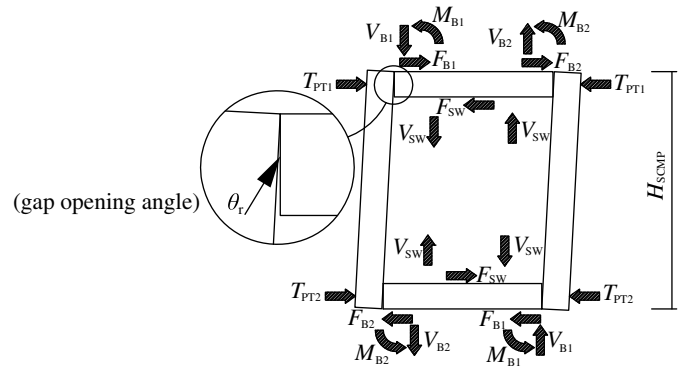


Fig. 2. Free-body diagram of deformed SCMP-SW

connected to the panel beams. As for the separated type of SCMP-SW, its free-body diagram is the same as the integrated type except for the elimination of  $F_{SW}$  and  $V_{SW}$  because the slit wall is placed in the other bay of the frame.

### SCMP-SW Response

Excluding the contribution from slit walls, SCMP exhibits a bilinear elastic behavior [Fig. 3(a)]. The initial stiffness,  $k_{i,PTF}$ , is equivalent to that of a frame with fully welded moment resisting connections, and the postdecompression stiffness reflects the reduced connection stiffness as the panel beam rocks about its flanges. From the free-body diagram, the recentering stiffness of a SCMP,  $k_r$ , can be calculated as (Clayton et al. 2012a)

$$k_r = \frac{4k_d^\theta}{H_{SCMP}^2} \quad (1)$$

where  $H_{SCMP}$  = overall height of the SCMP; and  $4k_d^\theta$  = sum of the postdecompression rotational stiffness of the PT connections in a SCMP, which may be calculated as (Garlock 2002; Clayton et al. 2012a)

$$k_d^\theta = \frac{H_{PB}^2}{2} \left( \frac{k_{PT}k_{PB}}{k_{PT} + k_{PB}} \right) \quad (2)$$

where  $H_{PB}$  = depth of the panel beam at the connection; and  $k_{PT}$  and  $k_{PB}$  = axial stiffness of all PT strands for each panel beam and axial stiffness of the panel beam, respectively.

The idealized hysteretic model of SWs is assumed to be an elastic-linear hardening backbone considering postyield stiffness ratio  $\alpha$  [Fig. 3(b)], with small compressive strength upon load reversal. Besides that, the reloading path always targets the previously

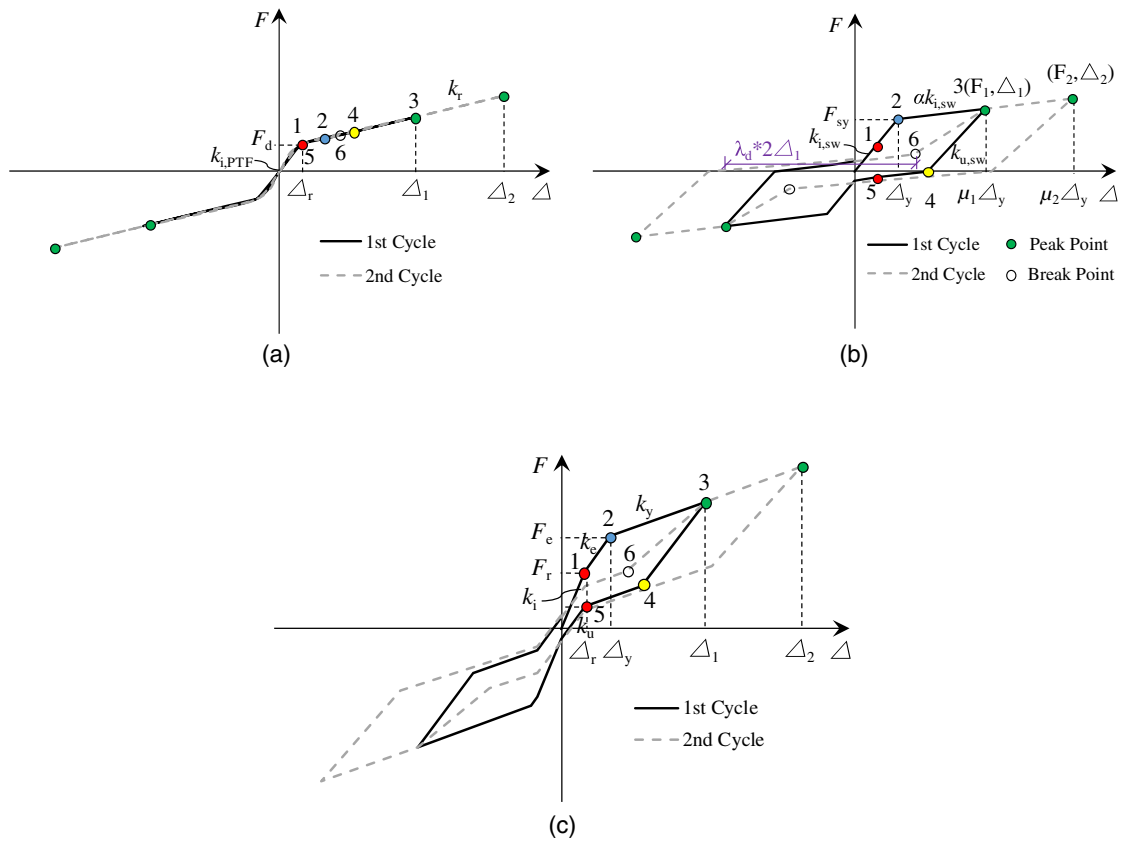


**Fig. 3.** (a) Idealized SCMP response; (b) idealized SW response; (c) idealized SCMP-SW response (significant events in the response history are indicated with number)

achieved maximum displacement point (Clough 1966). However, considering the pinching effect due to buckling of slit walls, the reloading path is usually separated into two branches by a break point (Ibarra et al. 2005). The break point is identified by a parameter  $\lambda_d$ , which defined the pinched displacement. For unloading, the stiffness  $k_{u,sw}$  is related to the initial stiffness  $k_{i,sw}$  by a ratio, which is expressed as a function of ductility demand and an unloading stiffness parameter  $\beta$

$$k_{u,sw} = k_{i,sw} \times \mu^{-\beta} \quad (3)$$

The parameters  $\lambda_d$  and  $\beta$  are kept constant as 0.8 and 0.2, respectively, which are based on the experimental results of the slit walls tested in this study.

The idealized lateral force versus displacement response of SCMP-SW [Fig. 3(c)] is a superposition of the individual response of the slit wall and SCMP, which is characterized by a flag-shaped hysteresis curve that is typical of self-centering systems. Here, partial strength of the SCMP-SW and the primary energy dissipation are provided by the slit walls, whereas the PT connections provide the recentering capability. During the initial lateral sway, SCMP-SW has a stiffness  $k_i$  equal to that of a conventional steel moment resisting frame combined with a slit wall placed inside. After gap opening (Event 1), the slit walls continue to resist additional load until yielding (Event 2), after which the lateral stiffness is substantially reduced. Upon unloading (Event 3), the elastic stiffness of the slit wall is partially recovered. After the slit walls are fully unloaded (Event 4), the PT connections recompress again with a recentering stiffness  $k_r$  (recompression at Event 5) and return to a zero force with a stiffness  $k_u$  (Clayton et al. 2012b). The initial lateral stiffness,  $k_u$ , will be retained at the beginning of subsequent load

cycles. After decompression, the SCMP-SW reload slowly until the break point of slit walls (Event 6) upon subsequent load cycles. The initial stiffness of SCMP-SW,  $k_i$ , equals the sum of initial stiffness of SCMP and lateral stiffness of the slit wall, that is

$$k_i = k_{i,PTF} + k_{i,sw} \quad (4)$$

### Posttensioned Connection Response

The PT connection behavior can be characterized by its moment versus gap rotation,  $\theta_r$ , response. An idealized PT connection response is shown in Fig. 4, where  $M_d$  is the decompression moment that can be calculated as (Dowden et al. 2012)

$$M_d = T_o \frac{H_{PB}}{2} \quad (5)$$

where  $T_o$  = initial PT force per panel beam. Event 1 (connection decompression) and Event 5 (connection recompression) shown in Fig. 4 represent the same definition as in Figs. 3(a and c). The idealized PT connection response loads and unloads along a bilinear elastic moment-gap rotation curve, while the initial stiffness is infinitely large and the postdecompression stiffness equals  $k_d^\theta$ .

### Experimental Tests of Full-Scale SCMP-SW Specimens

#### Test Setup

A picture and a schematic drawing of the test setup are shown in Figs. 5(a and b), respectively. The main frame had two bays and the

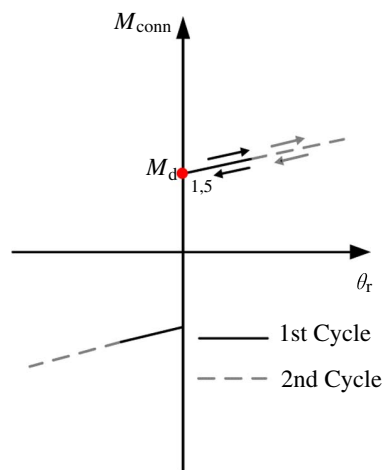


Fig. 4. Idealized PT connection response

SCMP was installed in the east bay through bolted connections at both ends of the panel beams, while the slit walls were either installed in the SCMP or the west bay. This full-scale specimen was part of a middle-height story taken from a prototype structure. The SCMP was measured as 2,680 mm long (edge-line panel-column dimension) and 3,000 mm in height (edge-line panel-beam dimension). The story height (through-beam centerline dimension) of the test specimen was 3,340 mm. A servohydraulic actuator was used to load the test specimen at a height of 3,490 mm from the lower flange of the bottom through beam. The bottom through beam, which was designed to simulate the boundary conditions for a middle-height floor, was connected to the reaction blocks using high-strength bolts at five different locations. There were two types of SCMP tested in this study, SCMP1 and SCMP2, and the differences between them are shown in Fig. 5(b).

Details of the SCMP-SW and its connection with the through beam are shown in Figs. 6(a–c). The PT strands were 15.2-mm-diameter 7-wire strands with an ultimate tensile strength of 1,860 MPa. Posttensioned strands were all placed symmetrically about the centerline of the panel beam within its depth, and typically anchored to the outer flanges of the panel columns with multi-strand barrel anchors. The PT strands were tensioned to 38% of their ultimate strength before the tests in order to provide sufficient self-centering capacity for SCMP while avoiding a PT strand yielding at 4% story drift based on design calculation. Because the stress level of the PT strands was increased along with the increasing story drift, higher initial PT strand stress might lead to premature failure of PT strands. Thus, the PT strands of SCMP could be reused in multiple tests without replacement. Horizontal stiffeners in the panel columns were added to protect against local failure due to large compressive forces acting on the flanges after decompression [Fig. 6(b)]. Transverse stiffeners were also included near the ends of the panel beams to prevent local buckling or damage caused by the forces exerted by the panel columns. A boundary plate was welded to the panel beam, while slit walls were connected to the boundary plate by connection plates using high-strength bolts. Circular holes that were 25 mm in diameter were created in the flanges of the panel columns and the transverse stiffeners of the panel beams to allow the PT strands to pass through. Filler plate was welded to the panel beam and extended to the outside of the end of the panel beam and a sloped cutout [Fig. 6(c)] was made in the overhang segment to avoid vertical sliding of the panel column when it was rocking about the panel-beam flange. Furthermore, the filler plate could also prevent the pounding between the outer

flange of the panel column and the lower flange of the through beam under large displacement of the frame. All the bolts were friction-type high-strength bolts of 20-mm diameter, and had a tensile strength of 1,000 MPa.

The section dimensions of the frame members and SCMP are listed in Fig. 7 and Table 1. The details of the slit wall are shown in Fig. 8 and the dimensions are listed in Table 2. The width-to-thickness ratio  $b/t$  of the flexural link is a key parameter in controlling the behavior of slit walls (Hitaka and Matsui 2003). There were four variants of slit walls in these tests in order to investigate the effects of various slit configurations on the slit walls and SCMP-SW responses. Lateral supports [visible in Fig. 4(a) but not shown in Fig. 4(b) for clarity] were provided to prevent out-of-plane movement of the main frame. Cover plates [Fig. 6(a)] were welded to the panel-beam flanges near the panel-beam ends to prevent displacement of the panel columns in both out-of-plane directions. Because the goal of these subassembly tests is to characterize the SCMP-SW and components behavior, complications in building applications such as gravity loads and the columns of upper floors were not considered.

### Specimen Descriptions

A total of nine specimens, listed in Table 3, were tested to investigate the behavior of SCMP-SWs. The naming convention for the test specimens is the kind of SCMP (e.g., S1), followed by the  $b/t$  ratio of flexural link of slit wall (e.g., W29). Specimen S0 only consisted of the 2-bay beam-through main frame, which was included to obtain the initial stiffness of the bare main frame. Tests S1 and S2 were done without any slit walls to ensure that the system exhibited the desired bilinear elastic response. The SCMP1 was placed into the east bay of the main frame for the specimens from S1 to S1W29, and the SCMP2 for the specimens from S2 to S2W36. The slit walls were only placed into the west bay for Specimen S2W36.

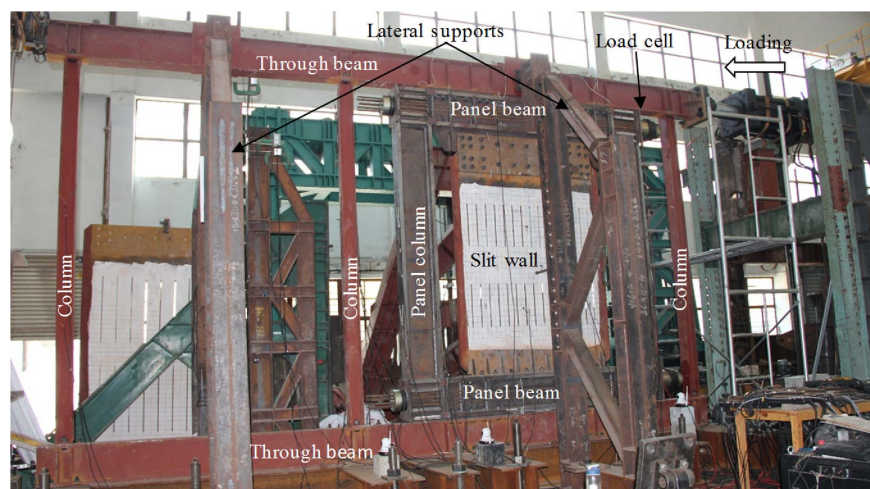
Specimens S1 and S2 were provided to investigate the effects of different SCMP parameters on the system response, especially the self-centering ability and initial stiffness. Specimens S2W29, S2W21, and S2W75 focused on the behavior of slit walls with varying slit patterns in terms of the slit design parameters  $b/t$  in order to understand how the slit configuration may influence the response of slit walls and system, especially the energy-dissipation ability.

Specimens S2W75(2) were provided to study the performance of after-test S2W75 with new slit walls and to verify its resilient functionality. The tests were conducted in the sequence as shown in Table 3. Specimens S0, S1, and S1W29 use the same main frame because it remains elastic in the test of Specimen S0 and S1, which was the same situation for Specimens S2 and S2W29. For Specimens S2W21 and S2W75, the main frames were all virgin specimens and had the same dimensions as that in Specimen S0. In all the tests except for S0, the PT strands of SCMP1 and SCMP2 were not retensioned after tests.

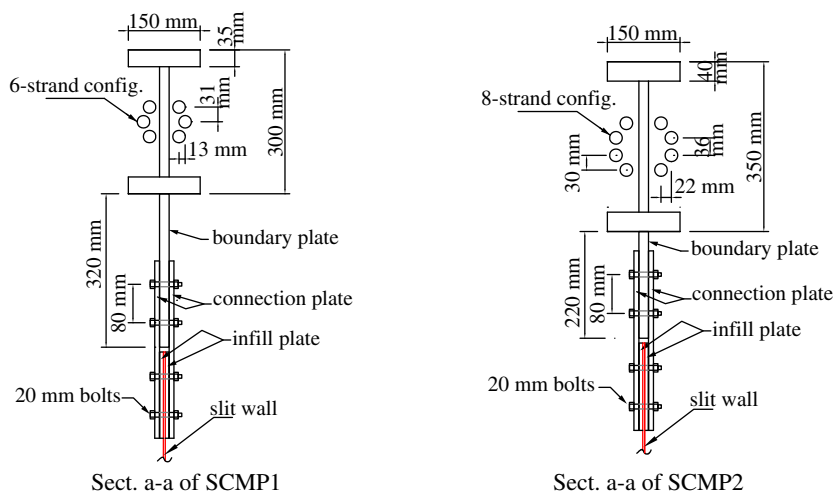
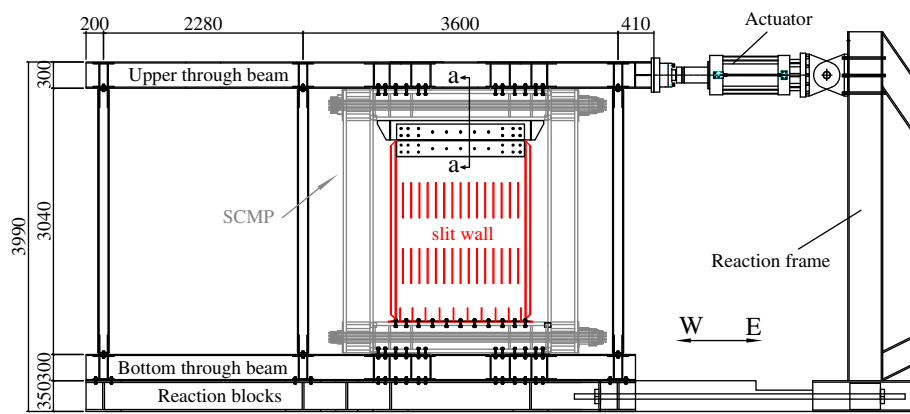
### Instrumentation

Instrumentation was installed to record the cyclic load response of the specimens, as well as the responses of panel beams, panel columns, connections, and slit walls. The applied load was measured directly from the actuator's load cell. Horizontal displacement transducers were placed at the middepth height of the through beams, at the upper flange at each end of the upper panel beam, and at the lower flange at each end of the lower panel beam to determine the through beams and panel beams displacements,





(a)



(b)

**Fig. 5.** (a) Picture and (b) schematic drawing of the SCMP-SW test setup

respectively. Displacement transducers were installed on the PT connections to measure the relative displacement between the extreme fiber of the panel-beam flange and the corresponding position of the panel column, from which the amount of the gap opening can be determined. Load cells were placed between the outer panel-column flange and the anchor to measure the resultant axial force of the PT strands per panel beam.

Numerous uniaxial strain gauges were installed at two sections along the through beams, columns, panel beams, and panel columns to determine the axial forces and bending moments of each member. The strain gauges were bonded parallel to the longitudinal axis of the members and on the outer faces of the flanges of the members. Rosette strain gauges were installed on the webs of the through beams, the ends of the columns in the beam-to-column

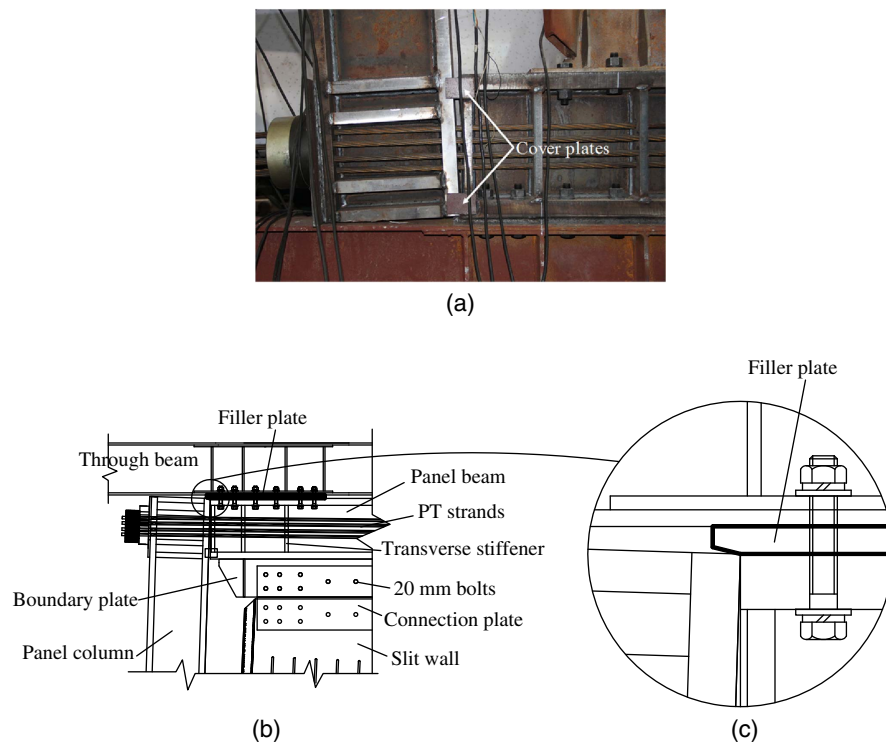


**Fig. 6.** Close-up view of SCMP-SW and its connection with frame through beam: (a) picture at 4% drift; (b) schematic drawing; (c) filler plate in the connection

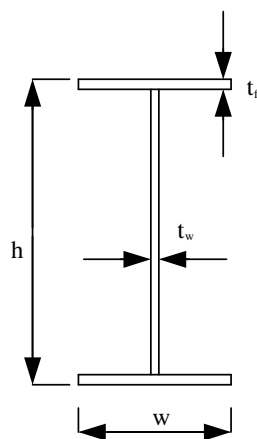


**Fig. 7.** Symbols of H-section dimensions

joints, and the corners of the slit walls to measure the local strains and to record the occurrence of yielding. The strain of the slit walls was measured through uniaxial strain gauges attached at the ends of flexural links between the slits to investigate its behavior under horizontal forces. The layout of displacement transducers and strain gauges for Specimen S2W75 is shown in Fig. 9.

### Material Properties

Coupon tests were conducted on materials taken from the members that may yield during the tests to determine their monotonic uniaxial material behavior (Table 4). Because the panel beams, panel columns, and PT strands are designed to remain elastic, no coupon tests were conducted on the materials. The member material

**Table 1.** Section Dimensions of the Frame Members and SCMP

Member	Section dimension $h \times w \times t_w \times t_f$ (mm)	Description
Column	$125 \times 125 \times 6.5 \times 9$	Hot-rolled H-section
Through beam	$300 \times 150 \times 10 \times 12$	Welded H-section
Panel beam of SCMP1	$300 \times 150 \times 20 \times 35$	Welded H-section
Panel column of SCMP1	$340 \times 150 \times 30 \times 35$	Welded H-section
Panel beam of SCMP2	$350 \times 150 \times 20 \times 40$	Welded H-section
Panel column of SCMP2	$340 \times 150 \times 30 \times 35$	Welded H-section

properties were taken as the averages from all the coupon tests for each member.

### Loading Protocol

The target cyclic drift history (Fig. 10) for the test is a modified version of the loading protocol given by ANSI/AISC 341-10 (AISC 2010b) with fewer cycles up to 1% story drift and the same number of cycles afterward. It is comprised of three cycles each to peak drift ratio of 0.225, 0.5, and 1%. After this the peak drift is increased to 1.5, 2, 3, and 4% each with two cycles of corresponding peak drift. In the cyclically symmetric loading protocol, an initial three cycles of pregap opening drift (0.225%) were imposed. Specimen S0 was tested solely for the purpose of getting the initial stiffness and would be reused in the following test so its loading program only consists of one cycle to the peak drift of 1% with all members remaining elastic. Because other studies suggest that the PT stress loss was a result of seating of the PT strand anchorage (Clayton et al. 2012b), Specimens S1 and S2 were tested to ensure that the system exhibited the desired bilinear elastic response and to measure the prestress loss, so their loading program only increases

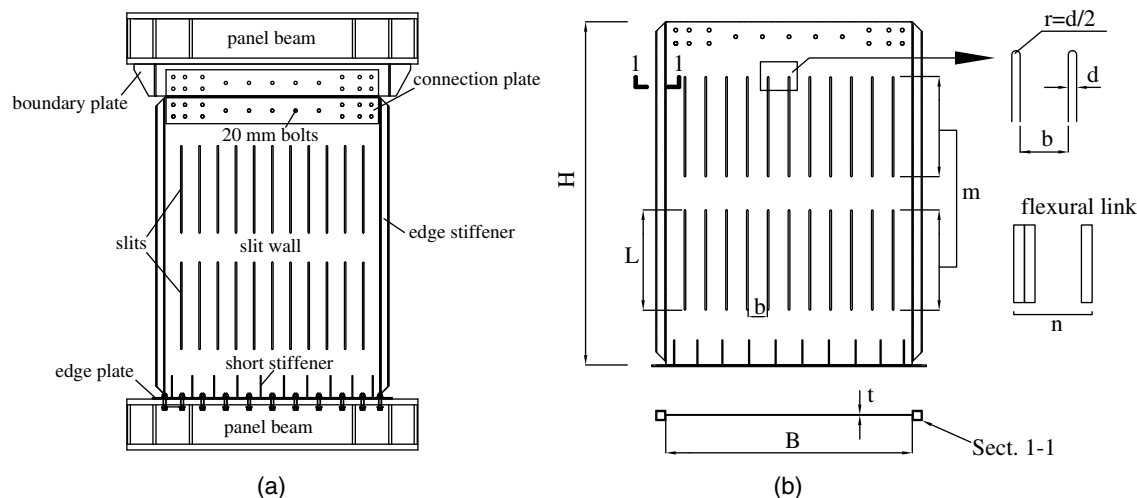


**Fig. 8.** Details of slit wall: (a) schematic drawing; (b) symbols of dimensions

**Table 2.** Dimensions of Slit Walls

Slit wall	$b/t$	$H$ (mm)	$B$ (mm)	$t$ (mm)	$b$ (mm)	$L$ (mm)	$m$	$n$	$d$ (mm)	Section 1-1 (mm)
W29	29	2,060	1,480	4	115	600	2	12	10	$60 \times 60 \times 6$
W21	21	2,060	1,480	4	84	400	2	16	10	$60 \times 60 \times 6$
W75	75	2,060	1,480	4	300	1,500	1	5	10	$60 \times 60 \times 6$
W36	36	2,700	1,500	4	144	720	2	10	10	$80 \times 80 \times 8$

**Table 3.** Specimen Descriptions

Specimen	SCMP	$b/t$
S0	—	—
S1	SCMP1	—
S1W29	SCMP1	29
S2	SCMP2	—
S2W29	SCMP2	29
S2W21	SCMP2	21
S2W75	SCMP2	75
S2W75(2)	SCMP2	75
S2W36	SCMP2	36

to the peak drift of 2 and 3%, respectively, with all members remaining elastic.

## Tests Results and Discussions

### Cyclic Load Response of Specimens

#### General Behavior

The base shear versus lateral drift responses of the system for each specimen are shown in Fig. 11. Specimen S0 had a linear elastic response with almost no energy dissipation. In general, the specimens with SCMP-SW exhibited the expected flag-shaped hysteresis. For Specimen S2W36, the flag-shaped system response was a combination of the bilinear response of SCMP2 and the response of the slit walls in the west bay of the main frame. No strength degradation was observed even at 4% drift for all specimens when the test was terminated. In all the tests except for Specimen S0, the gap

opening occurs near 0.3% drift before significant development of slit wall forces. Significant slit wall yielding was typically observed near 0.6% drift, as indicated by the reduction in specimen stiffness. Slit walls with a relatively large  $b/t$  ratio (e.g., W75) suffered pinched hysteresis when inner flexural links buckled out of plane and each link twisted in a similar manner to lateral-torsional buckling of beams. On the other hand, slit walls with a relatively small  $b/t$  ratio (e.g., W21) experienced a transverse (out of plane) deformation mode of the whole panel, similar to the shear buckling mode of steel plate walls. At large drifts, slit walls saw fracture that initiated at the end of slits. Cracks initiated at the slit end in W29 at 2% drift and gradually grew in length up to 30 mm without causing significant strength degradation. The tearing at the slit end locations is believed to be caused by the severe plastic deformation and exacerbated by the twisting of flexural links.

#### Posttensioned Strand Behavior

The response of the PT strands per panel beam begins with a resultant initial pretension force,  $T_o$ . When the system is loaded laterally, the tension force in the PT strands increases linearly as the gap rotation,  $\vartheta_r$ , increases. Upon unloading and recompression of the connections, the PT strands should return to their initial force,  $T_o$ , if there is no prestress loss (Clayton et al. 2012b). The target value of  $T_o$  was 600 kN for SCMP1 and 800 kN for SCMP2. However, the actual values obtained from the load cells were lower due to the limitation of the pretension equipment. For the same reason, the initial PT force  $T_o$  in the upper panel beam of SCMP2 was found to be larger than that in the bottom panel beam, while the initial PT force  $T_o$  for the upper panel beam of SCMP1 was found to be smaller than that for the bottom panel beam.

The cyclic response of the PT strands at the upper and bottom panel beams are shown for each specimen in Fig. 12. The measured PT force curves agree with the expected behavior; however, they show some loss of prestress, which results from seating of the PT strands anchorage during each cycle of loading. The maximum loss of prestress accumulated through all the tests was approximately 28% of the initial PT force. Fig. 12 also shows almost no prestress loss for the specimens from S2W29 to S2W36. This is because in all specimens only the main frame is changed while the PT frame of SCMP2 remains the same without retensioning of the PT strands after tests. Owing to the short PT strand length in SCMP1 and SCMP2, the prestress loss is so significant that a reduction coefficient for the PT force should be considered in the design of SCMP.

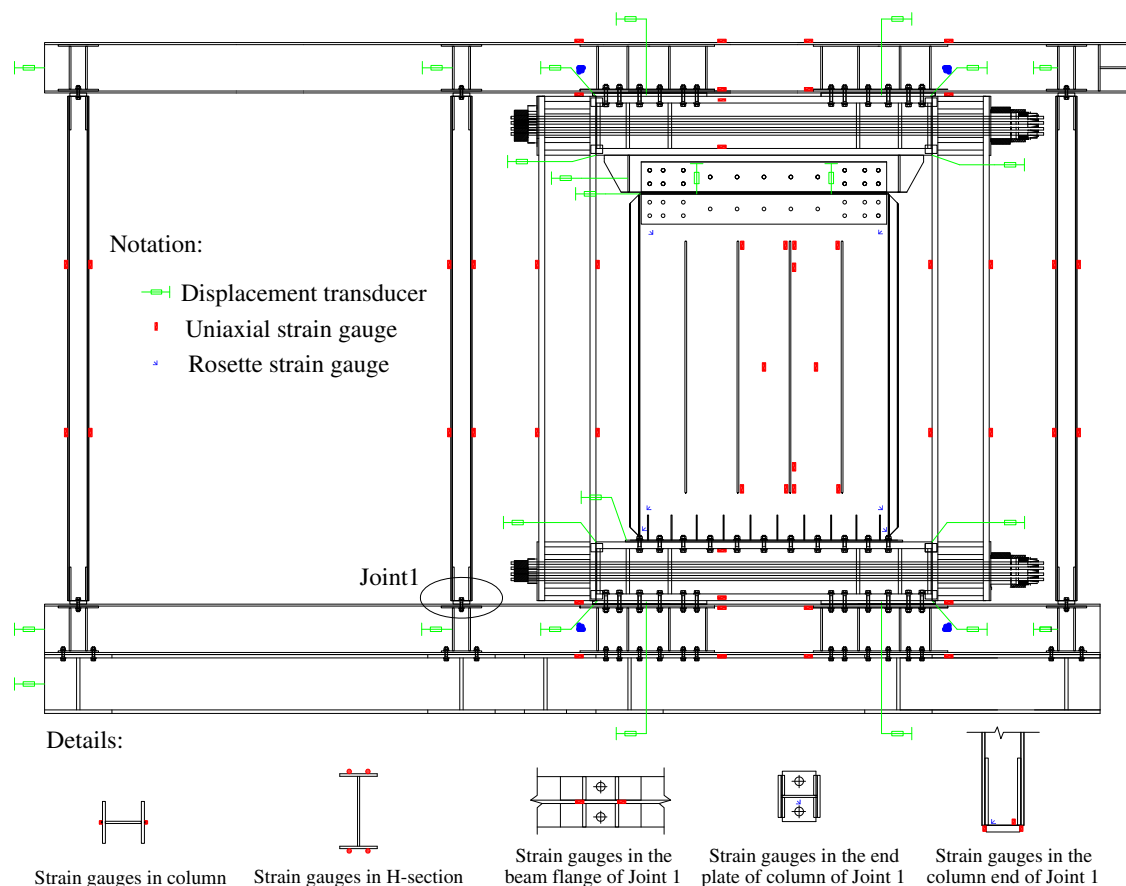


**Fig. 9.** Instrumentation layout of displacement transducers and strain gauges for Specimen S2W75

**Table 4.** Material Properties

Member	$\sigma_y$ (MPa)	$\sigma_u$ (MPa)	Descriptions
SW	313	541	Slit walls
TB-F	381	628	Flange plates of through beams
TB-W	377	645	Web plates of through beams
COL-F	403	675	Flange plates of columns
COL-W	399	629	Web plates of columns

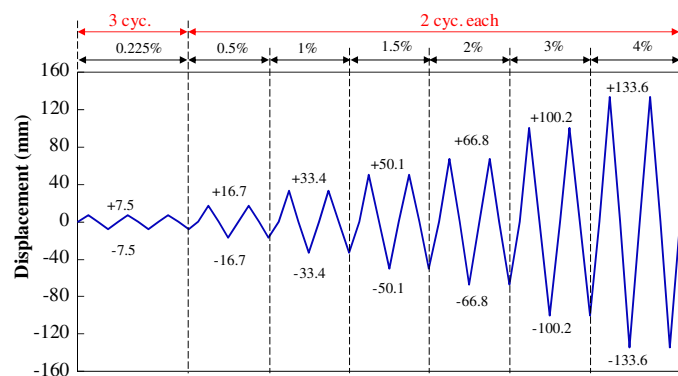


**Fig. 10.** Loading history

### Posttensioned Connection Behavior

The strain measurements from the sections at the third points of the panel columns were used to determine the axial forces and bending moments. The strain data collected from strain gauges indicate very

small strains owing to the large cross-sectional dimensions of the panel columns.

The bending moment in the PT connection can be derived using the shear force of the panel column. Here the inflection point of the panel column is assumed to be the middle height point. This assumption was made to determine the connection moment versus rotation responses for the PT connections at the east end of the panel beams for Specimen S2W36 (Fig. 13). The PT connection response of the other specimens was very close to the results shown in Fig. 13. The gap rotation was obtained from the data of displacement transducers installed at the PT connection. The PT connection behavior shown in Fig. 13 is consistent with that shown in Fig. 4. According to Eq. (5), the theoretical decompression moments of the PT connection for the upper and bottom panel beams of SCMP2 are 104.3 and 99.2 kN · mm, respectively, which overestimate the decompression moments. This overestimation might be caused by the uneven bearing surfaces at the panel-beam end and panel-column flanges due to construction tolerances.

### Slit Wall Behavior

The slit walls primarily resist the lateral loading through bending resistance of flexural links between slits and dissipate energy through inelastic action at the top and bottom of flexural links. The thin slit wall is assumed to have low buckling strength and therefore has small stiffness after unloading. The idealized hysteretic model of slit walls is assumed to be an elastic-linear hardening backbone.

The actual slit wall behavior [Fig. 14(b)] observed in the experiments looks similar to the idealized slit wall behavior in Fig. 3(b). First, the slit wall was able to resist load after yielding, with a small



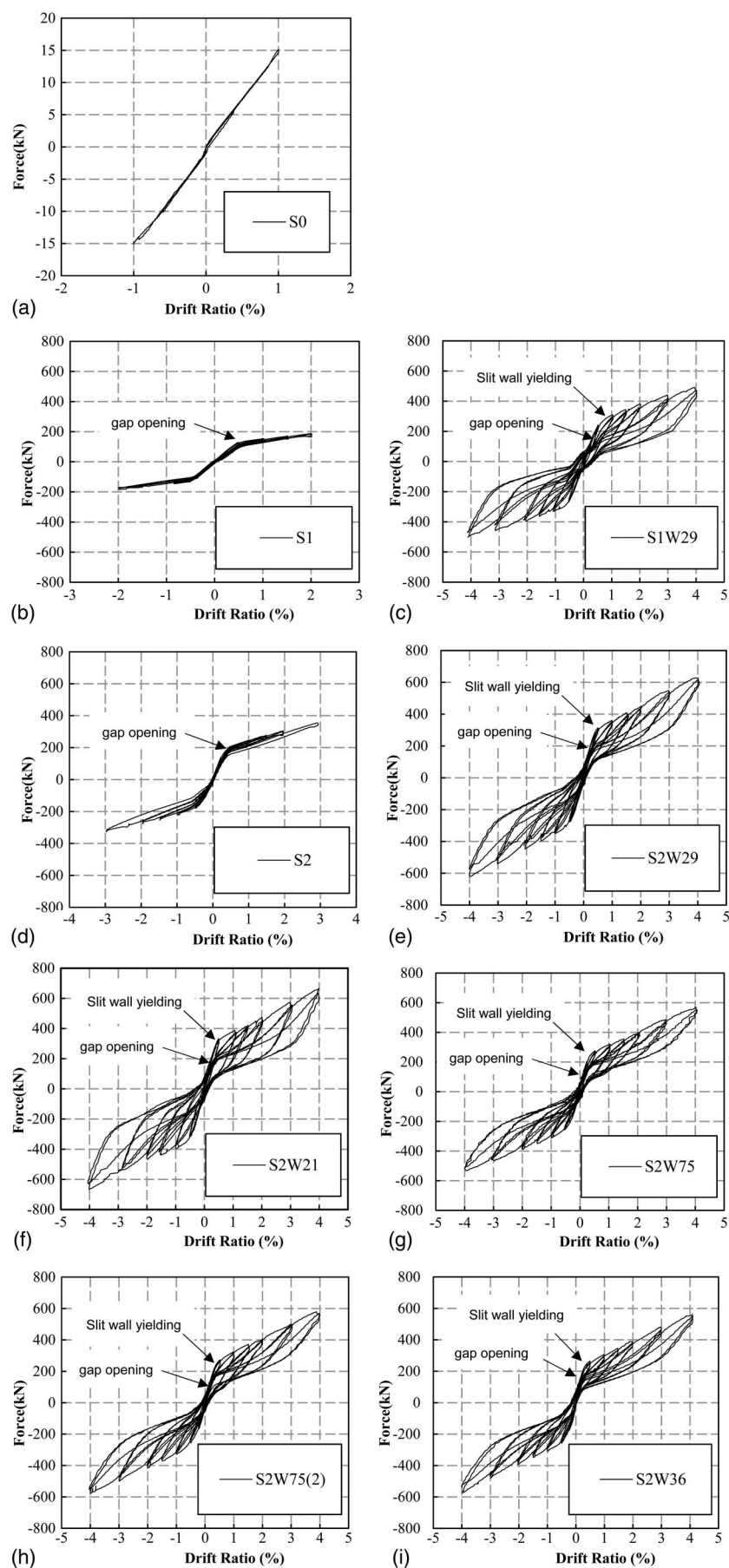


**Fig. 11.** Hysteresis curves of base shear versus drift ratio response of test specimens: (a) S0; (b) S1; (c) S1W29; (d) S2; (e) S2W29; (f) S2W21; (g) S2W75; (h) S2W75(2); (i) S2W36

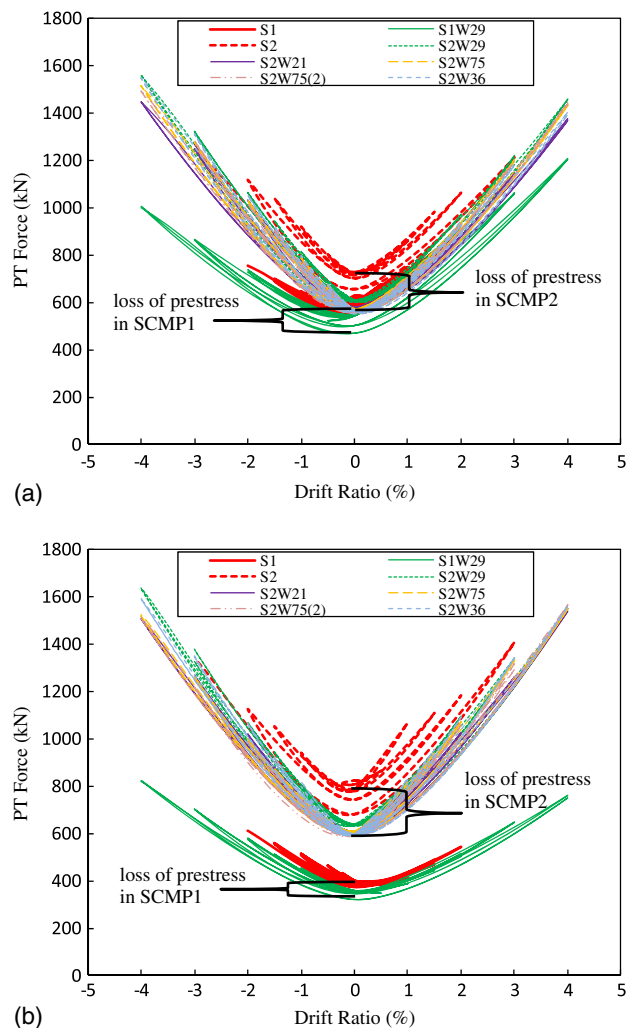


**Fig. 12.** Measured PT forces in all specimens: (a) upper panel beam; (b) bottom panel beam

postyielding stiffness, which is verified by comparing the hysteretic curves of Specimens S1 and S1W29 [Fig. 14(a)]. However, the compressive strength [see Fig. 14(a) for definition of compressive strength] of the three slit walls with different  $b/t$  ratios in Specimens S2W29, S2W21, and S2W75 were varying. The compressive strength here refers to the residual compressive load capacity of the slit wall once the load direction is reversed. The compressive strength of the slit walls was significant, as denoted

in Fig. 14(a), which might affect the recentering capability of SCMP-SW after system unloading (i.e., residual deformation might result from large residual compressive strength of SWs). Thus the compressive strength seemed to have an effect on the residual drift of the SCMP-SW. This yields different residual drift because the recentering ability of SCMP2 was consistent in those three specimens.

### Recentering Capabilities

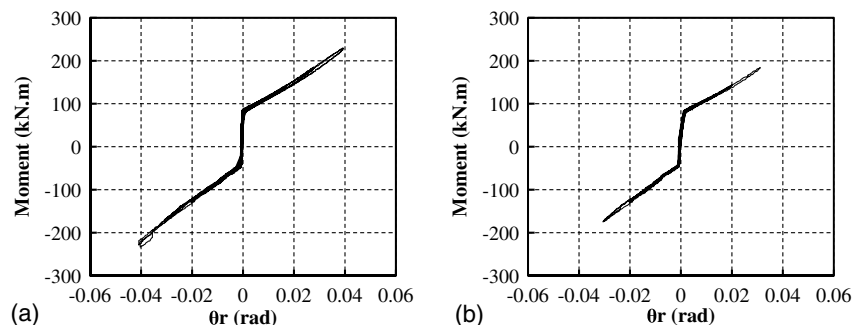
To assess the recentering capability in the specimens under the design-basis earthquake (DBE) and extreme earthquake loading, the residual drifts (i.e., drifts still remaining even after the actuator force was zeroed) of the specimens were determined following both positive and negative loading at the 2% (ASCE 2010) and 4% drift cycle, respectively. The results are shown in Table 5. Clayton et al. (2012b) proposed that remaining drifts less than 0.2% are considered to be recentered because this corresponds to out-of-plumb tolerances used in construction according to AISC 303-10 (AISC 2010a).

Table 5 shows that all specimens were able to recenter after the 2% drift cycle, with the exception of the positive loading of Specimen S1W29 and the negative loading of Specimen S2W21. Similarly, all the specimens could recenter after the 4% drift cycle, with the exception of Specimens S1W29 and S2W21, while the maximum residual drift was 0.34%, which slightly exceeded 0.2%. Specimen S1W29 had larger residual drift than Specimen S2W29 because the PT strands of SCMP1 were fewer than those of SCMP2. Specimens with smaller  $b/t$  ratios of slit walls had larger residual drifts owing to the additional lateral load resistance from the compressive strength of the slit wall during unloading. Here, greater stiffness of SCMP demands greater moment-resisting capacity of the through beam, which could be demonstrated by the data of the rosette strain gauges on the webs of the through beams in the panel-beam to through-beam connections.

Table 6 shows the experimental values of the initial stiffness and recentering stiffness of SCMP1 or SCMP2 in the specimens, obtained from a linear regression of the SCMP-SW responses shown in Fig. 10. The theoretical recentering stiffnesses,  $k_{r,th}$ , of SCMP1 and SCMP2 calculated from Eq. (1) are 1.06 and 2.02 kN/mm, respectively, which matches well with the experimental results.

### Effect of Varying Arrangement of Components

Fig. 15(a) shows the comparison of the system base shear versus lateral drift response of Specimens S1W29 and S2W29, the differences of which were the number of PT strands and dimensions of



**Fig. 13.** Moment versus rotation response of the east side PT connection in Specimen S2W36: (a) upper panel beam; (b) bottom panel beam

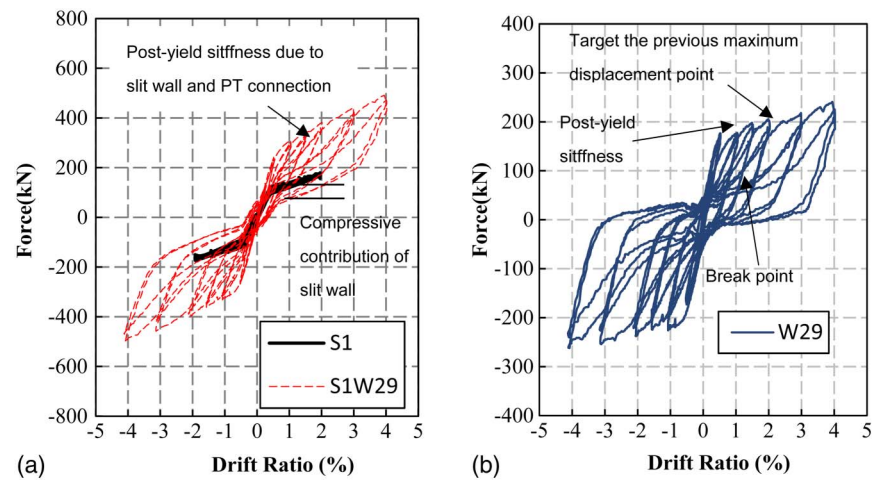


**Fig. 14.** (a) Hysteresis curves of test specimens with and without slit walls; (b) slit wall hysteresis curve

**Table 5.** Residual Drift Ratio after the 2 and 4% Drift Cycles in Percent

Specimen	After 2% cycle $k_i$ (kN/mm)		After 4% cycle $k_r$ (kN/mm)	
	Positive	Negative	Positive	Negative
S1	0.03	−0.04	—	—
S1W29	0.22	−0.20	0.34	−0.32
S2	0.02	−0.03	—	—
S2W29	0.04	−0.14	0.07	−0.20
S2W21	0.06	−0.24	0.08	−0.33
S2W75	0.03	−0.05	0.04	−0.15
S2W75(2)	0.03	−0.05	0.05	−0.16
S2W36	0.04	−0.07	0.03	−0.14

**Table 6.** Experimentally Measured Stiffness Values of SCMP-SW

Specimen	$k_{i,PTF}$ (kN/mm)	$k_r$ (kN/mm)	$k_i$ (kN/mm)
S1W29	7.44	1.08	14.85
S2W29	10.12	2.02	21.04
S2W21	10.34	2.23	22.44
S2W75	10.26	1.95	19.34
S2W75(2)	10.15	1.93	19.01
S2W36	10.18	1.96	—

panel beams in the SCMP. The experimental results demonstrate that the SCMP2 could provide larger stiffness and strength while giving the system larger recentering ability than SCMP1. The energy dissipation of the two specimens was almost identical due to the use of identical slit walls, which also suggests that the energy dissipation of the system is primarily provided by the slit wall.

Fig. 15(b) shows the system base shear versus lateral drift hysteresis curves of Specimens S2W29, S2W21, and S2W75, which have different width-to-thickness ratios for their slit walls. The experimental hysteresis curves suggest that the SCMP-SW with smaller  $b/t$  ratio of slit wall had larger stiffness, strength, and energy dissipation, meanwhile giving the system larger resistance to recentering during system unloading by larger residual drift.

Fig. 15(c) shows the system base shear versus lateral drift hysteresis curves of Specimens S2W75 and S2W75(2). The main frame of Specimen S2W75(2) was the reused one from Specimen

S2W75. The results in this figure show that owing to the SCMP the damaged frame system with new slit walls could provide almost identical performance in terms of stiffness, strength, and recentering ability compared with the original system. Therefore it can be concluded that the SCMP can potentially reduce the postearthquake structural repair workload demand.

Fig. 15(d) shows the system base shear versus lateral drift hysteresis curves of Specimens S2W75 and S2W36, the difference of which was the arrangement of SCMP and slit wall. The experimental curves show that the two types of SCMP-SWs with different arrangements of key components could provide the same stiffness, strength, and energy dissipation as well as recentering ability.

## Conclusions

Quasi-static cyclic loading tests were conducted on nine full-scale 1-story 2-bay through-beam frame specimens with SCMP-SW to investigate the system and SCMP-SW response behavior, the effects of the different slit configurations on slit wall response, and the effects of varying arrangements of the key structural components. The results of the experimental tests show that the beam-through frames with properly designed SCMP-SW are capable of providing satisfactory seismic resistance performance as well as recentering capacity while retaining the adjustable energy dissipation capacity provided by slit walls.

The examined configurations of the component arrangement include different locations of slit walls in the main frame. In the cases where slit walls were installed in the different bay as the separated type of SCMP-SW, the moment demands to the through beams were reduced significantly compared with the case in which the integrated type of SCMP-SW was used. The test results showed that the slit walls with smaller width-to-thickness ratios of flexural link provided larger stiffness, strength, and energy dissipation to the system, which may yield increased residual drift after system unloading. The tests also verified that due to the SCMP, after severe cyclic loading (at 4% drift) the system with newly replaced slit walls and a reused main frame was found to exhibit almost identical stiffness, strength, and recentering ability as the original system.

Furthermore, the results from all the tests suggest that the main frame with simple beam-to-column connections exhibits almost linear elastic behavior, and damage was only concentrated in the

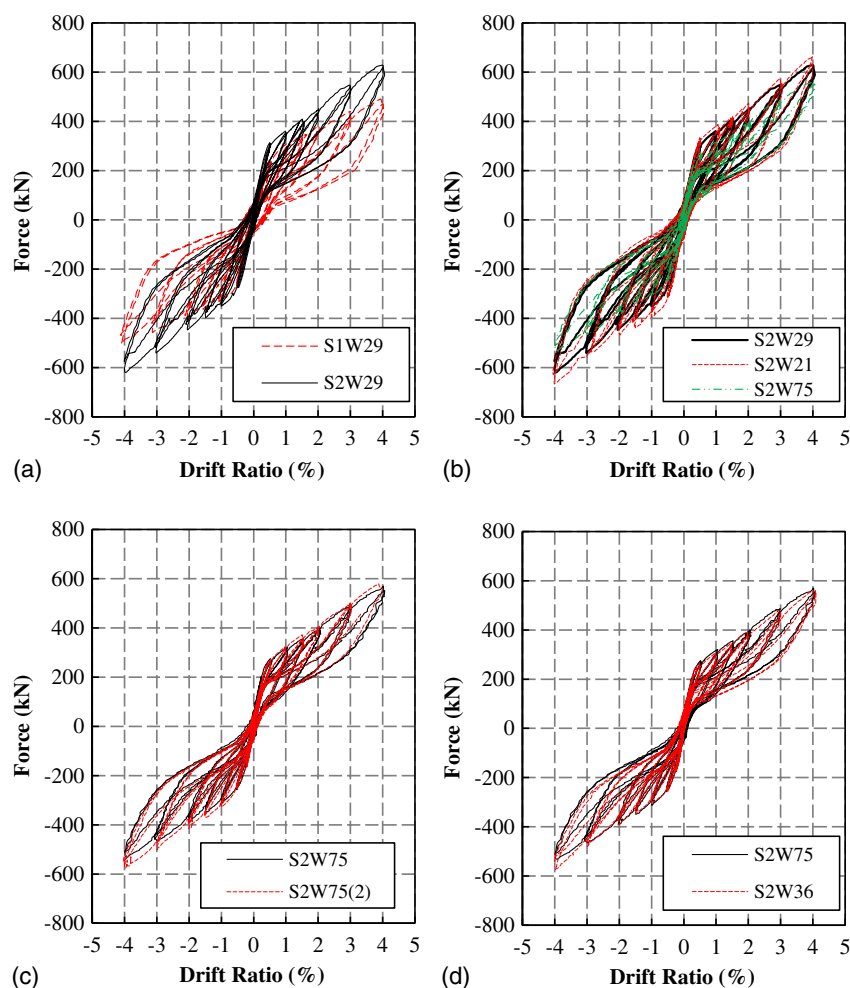


**Fig. 15.** Hysteresis curves of system base shear versus lateral drift ratio response of all test specimens

replaceable fuse elements (i.e., slit walls in this study) that can be easily replaced after earthquakes. Therefore, the SCMP-SWs are believed to offer a promising structural component that will be helpful to enhancing the seismic resilience of the beam-through steel frames and other types of structural systems. For example, SCMP-SW can be used as infill panels in seismic retrofitting of moment resisting frame structures.

## Acknowledgments

Financial support for this study was provided by the Natural Science Foundation of China (NSFC) with Grant No. 51778459, the State Key Laboratory of Disaster Reduction in Civil Engineering under Open Fund Award No. SLDRCE14-04, and “Shuguang Program” supported by Shanghai Education Development Foundation and Shanghai Municipal Education Commission. Any opinions, findings, conclusions, and recommendations presented in this paper are those of the writers and do not necessarily reflect the views of the sponsors.

## References

- AISC. (2010a). “Code of standard practice for steel buildings and bridges.” *AISC 303-10*, Chicago.
- AISC. (2010b). “Seismic provisions for structural steel buildings.” *ANSI/AISC 341-10*, Chicago.
- ASCE. (2010). “Minimum design loads for buildings and other structures.” *ASCE/SEI 7-10*, Reston, VA.
- Christopoulos, C., Filiatrault, A., and Folz, B. (2002a). “Seismic response of self-centering hysteretic SDOF systems.” *Earthquake Eng. Struct. Dyn.*, 31(5), 1131–1150.
- Christopoulos, C., Filiatrault, A., Uang, C. M., and Folz, B. (2002b). “Post-tensioned energy dissipating connections for moment-resisting steel frame.” *J. Struct. Eng.*, 10.1061/(ASCE)0733-9445(2002)128:9(1111), 1111–1120.
- Clayton, P. M. (2013). “Self-centering steel plate shear wall: Subassembly and full-scale testing.” Ph.D. dissertation, Univ. of Washington, Seattle.
- Clayton, P. M., et al. (2016). “Self-centering steel plate shear walls for improving seismic resilience.” *Front. Struct. Civil Eng.*, 10(3), 283–290.
- Clayton, P. M., Berman, J. W., and Lowes, L. N. (2012a). “Seismic design and performance of self-centering steel plate shear walls.” *J. Struct. Eng.*, 10.1061/(ASCE)ST.1943-541X.0000421, 22–30.
- Clayton, P. M., Berman, J. W., and Lowes, L. N. (2013). “Subassembly testing and modeling of self-centering steel plate shear walls.” *Eng. Struct.*, 56, 1848–1857.
- Clayton, P. M., Winkley, T. B., Berman, J. W., and Lowes, L. N. (2012b). “Experimental investigation of self-centering steel plate shear walls.” *J. Struct. Eng.*, 10.1061/(ASCE)ST.1943-541X.0000531, 952–960.
- Clough, R. W. (1966). *Effect of stiffness degradation on earthquake ductility requirements*, Univ. of California, Oakland, CA.
- Dowden, D. M., Purba, R., and Bruneau, M. (2012). “Behavior of self-centering steel plate shear walls and design considerations.” *J. Struct. Eng.*, 10.1061/(ASCE)ST.1943-541X.0000424, 11–21.



- El-Sheikh, M. T., Sause, R., Pessiki, S., and Lu, L.-W. (1999). "Seismic behavior and design of unbonded post-tensioned precast concrete frames." *PCI J.*, 44(3), 54–71.
- Fang, C., Wang, W., He, C., and Chen, Y. Y. (2017). "Self-centring behavior of steel and steel-concrete composite connections equipped with NiTi SMA bolts." *Eng. Struct.*, 150, 390–408.
- Fang, C., Yam, M. C. H., Lam, A. C. C., and Xie, L. K. (2014). "Cyclic performance of extended end-plate connections equipped with shape memory alloy bolts." *J. Constr. Steel Res.*, 94, 122–136.
- Fang, C., Yam, M. C. H., Lam, A. C. C., and Zhang, Y. Y. (2015). "Feasibility study of shape memory alloy ring spring systems for self-centring seismic resisting devices." *Smart Mater. Struct.*, 24(7), 075024.
- Garlock, M. (2002). "Design, analysis, and experimental behavior of seismic resistant post-tensioned steel moment resisting frames." Ph.D. dissertation, Lehigh Univ., Bethlehem, PA.
- Garlock, M., Ricles, J., and Sause, R. (2005). "Experimental studies of full-scale posttensioned steel connections." *J. Struct. Eng.*, 10.1061/(ASCE)0733-9445(2005)131:3(438), 438–448.
- Garlock, M., Sause, R., and Ricles, J. (2007). "Behavior and design of post-tensioned steel frame systems." *J. Struct. Eng.*, 10.1061/(ASCE)0733-9445(2007)133:3(389), 389–399.
- Hitaka, T., and Matsui, C. (2003). "Experimental study on steel shear wall with slits." *J. Struct. Eng.*, 10.1061/(ASCE)0733-9445(2003)129:5(586), 586–595.
- Ibarra, L. F., Medina, R. A., and Krawinkler, H. (2005). "Hysteretic models that incorporate strength and stiffness deterioration." *Earthquake Eng. Struct. Dyn.*, 34(12), 1489–1511.
- Kurama, Y., Sause, R., Pessiki, S., and Lu, L.-W. (1999). "Lateral load behavior and seismic design of unbonded post-tensioned precast concrete walls." *ACI Struct. J.*, 96(4), 622–632.
- Mutoh, K., Miyashita, O., Osada, M., and Kanayama, H. (1968). "Stress and deformation of slit wall, using FEM." *Summaries of Technical Papers of Annual Meeting, AIJ, Chugoku, Japan*, 543–544 (in Japanese).
- Omori, S., Toyama, K., Cho, T., and Takahashi, T. (1966). "Test on RC shear wall with slits." *Summaries of Technical Papers of Annual Meeting, AIJ, Chugoku, Japan*, 204–205 (in Japanese).
- Priestly, M. J. N. (1991). "An overview of PRESSS research program." *PCI J.*, 36(4), 50–57.
- Ricles, J., Sause, R., Peng, S., and Lu, L. (2002). "Experimental evaluation of earthquake resistant posttensioned steel connections." *J. Struct. Eng.*, 10.1061/(ASCE)0733-9445(2002)128:7(850), 850–859.
- Rojas, P., Ricles, J., and Sause, R. (2005). "Seismic performance of post-tensioned steel moment resisting frames with friction devices." *J. Struct. Eng.*, 10.1061/(ASCE)0733-9445(2005)131:4(529), 529–540.
- Wang, W., Chan, T. M., and Shao, H. L. (2015a). "Seismic performance of beam-column joints with SMA tendons strengthened by steel angles." *J. Constr. Steel Res.*, 109, 61–71.
- Wang, W., Chan, T. M., Shao, H. L., and Chen, Y. Y. (2015b). "Cyclic behavior of connections equipped with NiTi shape memory alloy and steel tendons between H-shaped beam to CHS column." *Eng. Struct.*, 88, 37–50.
- Wang, W., Du, X. L., Zhang, Y. F., and Chen, Y. Y. (2017). "Experimental investigation of beam-through steel frame with self-centering modular panels." *J. Struct. Eng.*, 10.1061/(ASCE)ST.1943-541X.0001743, 04017006.
- Wang, W., Fang, C., and Liu, J. (2016a). "Self-centering beam-to-column connections with combined superelastic SMA bolts and steel angles." *J. Struct. Eng.*, 10.1061/(ASCE)ST.1943-541X.0001675, 04016175.
- Wang, W., Zhou, Q., Chen, Y. Y., Tong, L. W., and Chan, T. M. (2013). "Experimental and numerical investigation on full-scale tension-only concentrically braced steel beam-through frames." *J. Constr. Steel Res.*, 80, 369–385.
- Wang, W., Zou, C., Chen, Y. Y., Zhang, Y. F., and Chen, Y. S. (2016b). "Seismic design of multistory tension-only concentrically braced beam-through frames aimed at uniform inter-story drift." *J. Constr. Steel Res.*, 122, 326–338.